Organic & Biomolecular Chemistry

Cite this: *Org. Biomol. Chem.*, 2011, **9**, 4550

www.rsc.org/obc

PAPER

Sequential catalytic role of bifunctional bicyclic guanidine in asymmetric phospha–Michael reaction†

Bokun Cho, Choon-Hong Tan and Ming Wah Wong*

Received 2nd February 2011, Accepted 23rd March 2011
DOI: 10.1039/c1ob05186e

The catalytic mechanism and origin of enantioselectivity of bicyclic guanidine-catalyzed phospha–Michael reaction between diphenyl phosphine oxide and β-nitrostyrene were investigated by DFT calculations at M06-2X/cc-pVTZ//M06-2X/cc-pVDZ level in conjunction with the implicit SMD solvation method. The catalyst is found to be involved in all 3 steps of the proposed catalytic cycle, namely (1) tautomerization of phosphine oxide, (2) C–P bond formation and (3) concerted hydrogen transfer. The bifunctional role of the guanidine catalyst is clearly demonstrated in all 3 key steps. Due to the geometry of the bicyclic guanidine catalyst, the preferred orientation of the reactants in the transition state of enantioselective C–P bond forming step favours the *R* enantiomer, in excellent accord with the observed enantioselectivity. Analysis of various transition states suggests that the asymmetric C–P bond formation is controlled by the hydrogen bonding interaction and steric effect between the catalyst and substrate. Various weaker C–H $\cdots$ X (X = N, O and π) interactions also play a role in stabilizing the key transition states.

Introduction

Phospha-Michael reaction represents one of the most important routes for constructing carbon-phosphorus bond in the synthesis of organophosphorus compounds.[1] The importance of organophosphorus compounds can be seen in its ubiquitous utility as reagents in organic synthesis,[2] nucleophilic[3] and Brønsted acidic[4] organocatalysts, chiral ligands for transition metals[5] and peptidomimetics.[6]

Organocatalysis provides an efficient approach to generate chiral organophosphorus compounds.[1a] Chiral guanidine catalysts are widely employed in asymmetric synthesis and their versatility can be seen from the wide range of reactions that they can catalyze.[7] Despite the planarity of the guanidine moiety, it can be functionalized to create the chirality required for asymmetric catalysis. The bicyclic guanidine scaffold is used extensively due to rigidity of the framework which eliminates isomerization of the guanidine and restricts rotational freedom.[8] Appropriate substituents can be introduced to bicyclic guanidine to induce asymmetry.

In 2007, we reported the use of a Brønsted base bicyclic guanidine catalyst for phospha–Michael reaction between aromatic phosphine oxides with nitrostyrene (Scheme 1).[9] Remarkable enantioselectivity of up to 99% *ee* has been observed, using 10 mol % catalyst loading. The robustness of this bicyclic guanidine catalyst has been demonstrated in a variety of asymmetric reactions.[10,11]

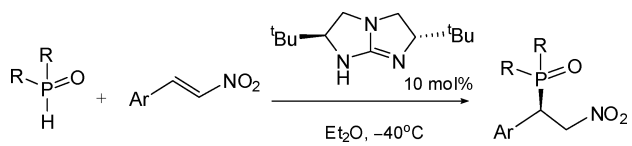

Scheme 1 Bicyclic guanidine-catalyzed phospha–Michael reaction of aromatic phosphine oxides with nitrostyrene reported by Tan *et al.*[9]

There are two plausible catalytic modes for guanidine catalysts: Brønsted basic and covalently-bonded nucleophilic pathways. For reactions such as the ring-opening polymerization of cyclic ester[12] and intramolecular aldol reaction,[13] both mechanisms are feasible and they have been elucidated *via* kinetics and theoretical studies to determine the preferred pathway.

The guanidine catalyst, bearing both Brønsted-acidic and basic sites, can activate both reaction substrates simultaneously. This bifunctional activation mode of guanidine catalyst was proposed

Department of Chemistry, National University of Singapore, 3 Science Drive 3, Singapore, 117543. E-mail: chmwmw@nus.edu.sg; Fax: +65 67791691; Tel: +65-65164320

† Electronic supplementary information (ESI) available: Total energies and optimized coordinates of all structures reported in text (Table S1), calculated structural parameters of α,α′,β-triphenyl substituted{5,5}-bicyclic guanidine (Table S2) Morokuma-Kitaura energy decomposition ananlyis (Tables S3-S5), hydrogen bonding properties (Table S6), concerted transition state of uncatalyzed-phospha-Michael reaction (Fig. S1), steric constraint of **TS2** in alignment B (Fig. S2), comparison of *R*-**TS2a** and *S*-**TS2j** (Fig. S3), accessibility of β-carbon in s-*cis* and s-*trans* hydrogen bonding (Fig. S4) and **TS2** transition states with monodentate hydrogen bond (Fig. S5). See DOI: 10.1039/c1ob05186e

initially by Corey *et al.*[14] in bicyclic guanidine-catalyzed Strecker reaction. This hypothesis was subsequently supported by theoretical calculation.[15] In a recent combined experimental and theoretical study of bicyclic guanidine-catalyzed conjugate addition of fluorocarbon,[11] the bifunctional activation mode of the guanidine catalyst was further established. The strong Brønsted basicity of guanidine deprotonates and activates the nucleophile while the Brønsted acidity of the N–H moiety increases the electrophilicity of the electrophilic substrate. Experimentally, the bifunctionality of guanidine molecules is supported by the observation of two chloride complexes with cyclic bicyclic guanidinium ion.[16] To further shed light on the role of the bicyclic guanidine catalyst and the origin of the observed high enantioselectivity, density functional theory (DFT) calculations have been performed on the phospha–Michael reaction between diphenyl phosphine oxide and β-nitrostyrene using the bicyclic guanidine catalyst (Scheme 1). The factors influencing the enantioselectivity of the reaction were explored through studying various transition states involved in the catalytic reactions.

Computational methods

Geometry optimizations of equilibrium structures and transition states related to the bicyclic guanidine-catalyzed phospha-Michael reaction were performed using a hybrid *meta* exchange–correlation functional M06-2X, developed by Zhao and Truhlar,[17] together with the cc-pVDZ[18] basis set. The M06-2X functional was chosen as this empirical functional is better suited than normal hybrid DFT methods (*e.g.* B3LYP) in handling kinetics, thermodynamics, and noncovalent interactions. This DFT method has been applied successfully to investigate the mechanisms of several catalytic organic reactions.[19] Higher-level relative energies were computed using a larger cc-pVTZ basis set based on the M06-2X/cc-pVDZ optimized geometries. Frequency analyses were performed on the M06-2X/cc-pVDZ optimized geometries to confirm the nature of the stationary points as equilibrium structures (with all real frequencies) or transition states (with only one imaginary frequency). The effect of solvation was examined by a continuum solvation model SMD,[20] which solves the nonhomogeneous Poisson equation for the bulk electrostatic contribution using a self-consistent reaction field treatment. This solvation method uses it customized set of solute radii and the cavitation and dispersion interactions employ a sum of terms proportional to the solvent accessible surface area.[20] The solvation energies were obtained at the M06-2X/cc-pVTZ level in diethyl ether solvent ($\varepsilon = 4.24$), based on the gas-phase optimized geometries. Unless otherwise noted, the relative free energies (in kJ mol^{-1}) reported in the text correspond to Gibbs free energies at 233 K, the temperature at which the phospha-Michael reaction was carried out,[9] in diethyl ether solvent. These solution-phase free energies include the solvation and dispersion contributions together with entropy term. Charge density analysis (at M06-2X/cc-pVTZ level) based on the atom in molecule (AIM)[21] approach was performed using the MORPHY 98 program.[22] All DFT calculations were performed using the Gaussian 09 suite of programs.[23] Morokuma-Kitaura energy decomposition analysis[24] was calculated using the GAMESS program [25]

Results and discussion

Proposed catalytic cycle

The active intermediate to initiate the nucleophilic attack from the phosphorus is believed to be phosphinic acid.[26] Our recent theoretical study has demonstrated the bifunctional activation mode of bicyclic guanidine catalyst in conjugate addition of fluorocarbon.[11] For the phospha–Michael reaction investigated here, we envisage a similar bifunctional role of the bicyclic guanidine catalyst in all 3 stages of our proposed catalytic cycle (Fig. 1): (1) tautomerization of phosphine oxide to phosphinic acid, (2) simultaneous C–P bond formation between phosphinic acid and nitrostyrene and proton abstraction of phosphinic acid by the guanidine catalyst, and (3) concerted hydrogen transfer of the nitronate guanidinium intermediate to yield the Michael addition product and regeneration of the guanidine catalyst. The key transition states involved in the 3 catalytic stages are **TS1**, **TS2** and **TS3**, respectively (Fig. 1). In each stage, the bicyclic guanidine catalyst serves as a Brønsted base and a Brønsted acid simultaneously in the transition state. It is important to note the guanidine catalyst forms a hydrogen-bonded pre-transition state complex (**1**) with phosphine oxide in the initial stage.

Tautomerization of phosphine oxide to phosphinic acid

It is instructive to first examine various plausible reaction pathways for tautomerization of phosphine oxide to phosphinic acid. Three possible pathways have been considered: (i) direct intramolecular 1,2-hydrogen shift (*i.e.* uncatalyzed tautomerization); (ii) concerted intermolecular hydrogen transfer *via* a dimer of phosphine oxide; and (iii) guanidine-catalyzed tautomerization. The direct intramolecular hydrogen transfer [pathway (i)], *via* transition state **TS4** (Fig. 2), is calculated to have a very high activation barrier of 249 kJ mol^{-1}. Previous theoretical study has shown that such 1,2-H migration to be a forbidden process.[27] For the second tautomerization pathway, phosphine oxide initially forms a dual hydrogen-bonded dimer (Fig. 2). Simultaneous intermolecular hydrogen transfer of this dimer, *via* transition state **TS5**, leads to 2 molecules of phosphinic acid. This intermolecular process has a significantly lower barrier of 117 kJ mol^{-1}, compared to the direct intramolecular 1,2-H shift pathway.

For the guanidine-catalyzed tautomerization [pathway (iii)], phosphine oxide first coordinates with the bicyclic guanidine catalyst to yield a stable dual hydrogen-bonded complex **1** (see Fig. 2). The guanidine catalyst provides simultaneously a proton donor (*i.e.* N–H) and a proton acceptor (*i.e.* nitrogen lone pair) in the complex. This pre-transition state complex brings the phosphine oxide close together for the subsequent concerted intermolecular hydrogen transfer, *via* transition state **TS1** (Fig. 2), to yield a tautomer guanidine complex **2**. This step involves a simultaneous hydrogen abstraction from the phosphine oxide (P–H) by the catalyst and hydrogen donation from the catalyst (N–H) to the oxygen moiety of the phosphine oxide. This catalyzed tautomerization process is predicted to have the lowest activation barrier of 57 kJ mol^{-1}. Hence, we conclude that the bicyclic guanidine plays a vital role in the first stage of the catalytic cycle in converting phosphine oxide to phosphinic acid for the subsequent C–P bond formation.

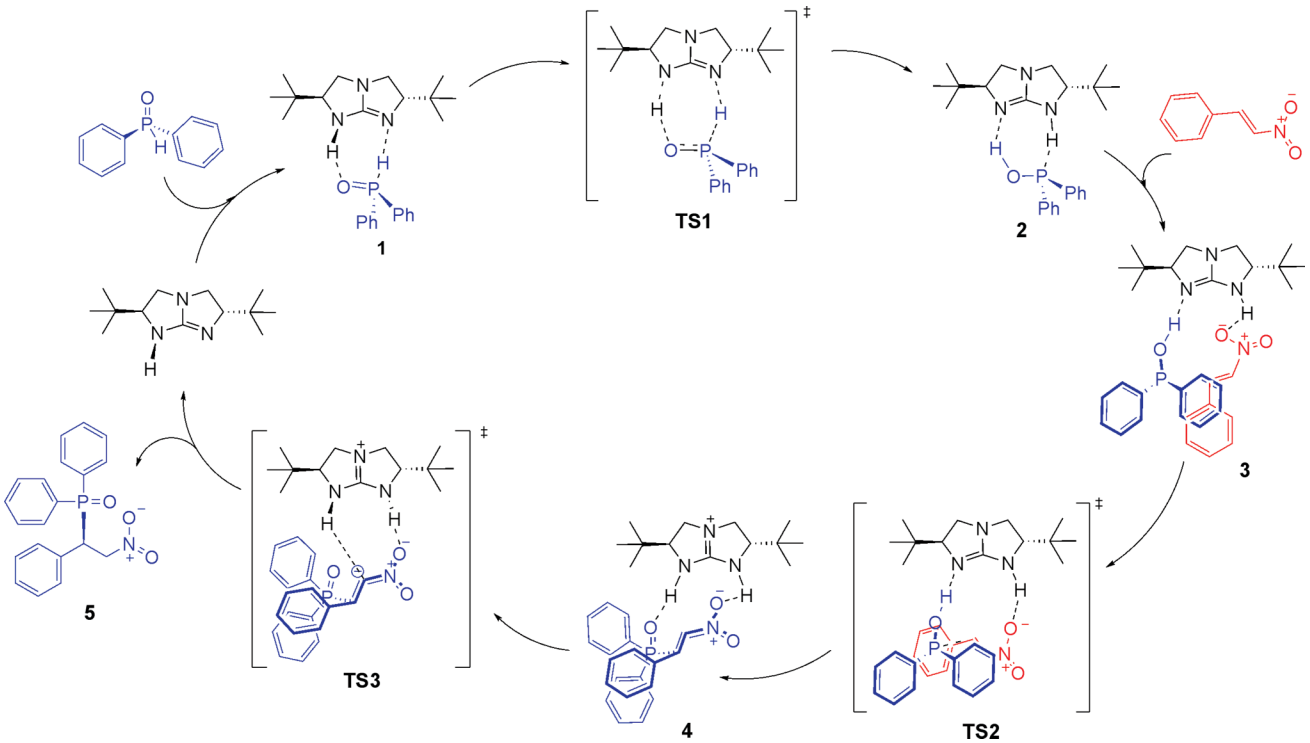

Fig. 1 Proposed catalytic cycle of bicyclic guanidine catalyzed-phospha Michael reaction between diphenyl phosphine oxide and β-nitrostyrene.

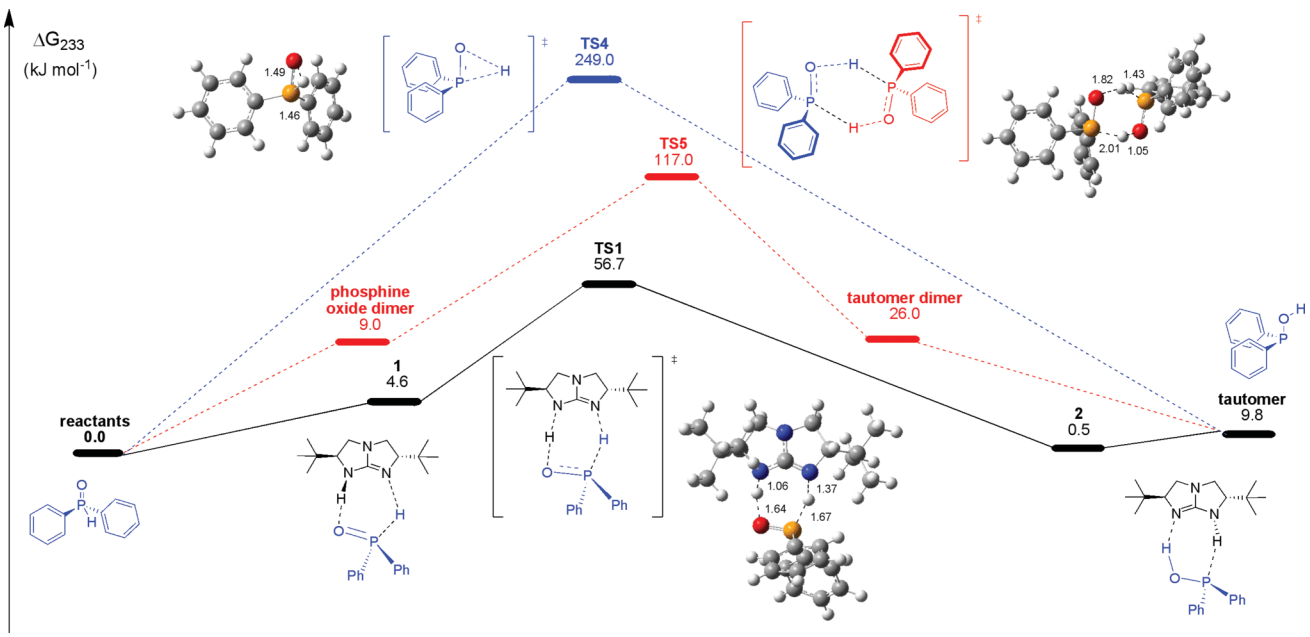

Fig. 2 Schematic potential energy diagram of various tautomerization pathways of phosphine oxide. Calculated relative free energies in diethyl ether solvent were obtained at SMD-M06-2X/cc-pVTZ//M06-2X/cc-pVDZ level.

Enantioselectivity in the carbon-phosphorus bond formation

In the second stage of the catalytic cycle, the phosphinic acid-guanidine complex **2** interacts with nitrostyrene to from an intermediate complex **3**, which is stabilized by dual hydrogen bonds and $\pi\cdots\pi$ interaction between nitrostyrene and phosphinic acid (see Fig. 3). The interaction distance between the 2 aromatic rings is ~3.25 Å. This pre-transition state complex (**3**) serves an essential role of bringing the Michael donor and acceptor to close proximity with the correct orientation for the carbon-phosphorus bond formation process, *via* transition state **TS2** (Fig. 1). This transition state involves a concerted C–P bond formation and proton abstraction of phosphinic acid by the guanidine catalyst, which leads to an ion-pair complex **4** (Fig. 1) between the phosphine oxide nitronate ion intermediate and the guanidinium catalyst.

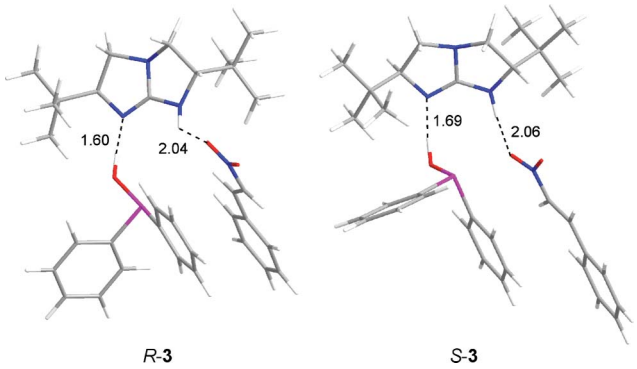

Fig. 3 Optimized (M06-2X/cc-pVDZ) geometries of intermediate complexes *R*-**3** and *S*-**3**. Hydrogen bond distances are given in Å.

The effect of the bifunctionality of the guanidine catalyst can be seen in the HOMO and LUMO energies of the reactants and pre-transition state complex **3**. The guanidine catalyst raises the HOMO of the phosphinic acid tautomer by 0.61 eV (for both *R*-**3** and *S*-**3**), which activates the nucleophile. Concurrently, the catalyst lowers the LUMO of nitrostyrene by 0.12 eV (for both *R*-**3** and *S*-**3**), which increases the electrophilicity of nitrostyrene. The HOMO and LUMO of *R*-**3** are depicted in Fig. 4. This dual activation facilitates the electron transfer in the C–P bond forming process. The bicyclic guanidine catalyst serves as hydrogen-bond donor and acceptor with both Michael donor and acceptor substrates.

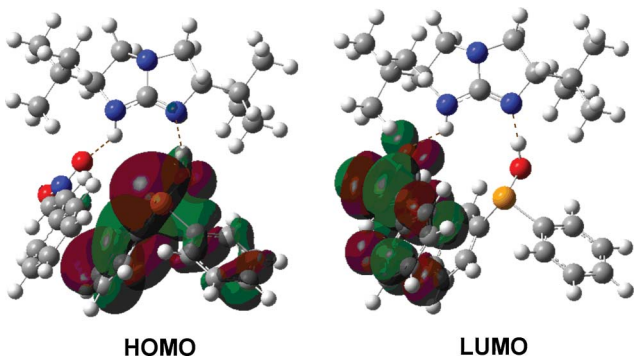

Fig. 4 HOMO and LUMO of pre-transition state complex *R*-**3**.

The C–P bond forming step dictates the enantioselectivity of the phospha–Michael reaction. Thus, various **TS2** transition states provide the key to understand the overall stereoselectivity of the reaction. Here, we designate *R*-**TS2** and *S*-**TS2** for transition states leading to *R*- and *S*-products, respectively. Nitrostyrene has one pro-chiral center and the nucleophile (Michael donor) attack from *Re*- or *Si*-face will afford *R*- or *S*-product, respectively.

Let us begin by examining how the Michael donor and acceptor and the bicyclic guanidine catalyst would assemble in the C–P bond forming transition state (*i.e.* **TS2**). The symmetry and chirality of the guanidine catalyst can be visualized with reference to the plane of the bicyclic ring. In the optimized geometry of the bicyclic guanidine, the acidic N–H proton is significantly nonplanar and orientated away from the neighbouring *t*-butyl group (Fig. 5). This structural feature is observed in the X-ray crystal structure of α,α′,β-triphenyl substituted{5,5}-bicyclic guanidine, synthesized by Ishikawa *et al.*[28] The geometry

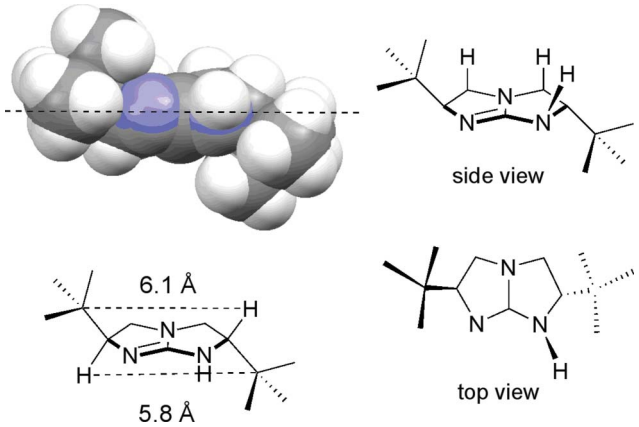

Fig. 5 Geometry of the bicyclic guanidine catalyst.

of this bicyclic guanidine crystal is readily reproduced by the M06-2X/cc-pVDZ level of theory, with small mean unsigned error for the computed bond lengths and bond angles (Table S2, ESI†). In particular, the orientation of the N–H proton is reproduced. It is important to note that the face containing the N–H proton is sterically less hindered than the opposite face, by comparing the distances between the α hydrogen and the tertiary carbon of the opposite *t*-butyl group (see Fig. 5). Thus, the bicyclic guanidine molecule is slightly distorted from the expected C_2 symmetry. The orientation of the N–H acidic proton and the differential face crowding are important factors influencing the asymmetry of the enantioselective step.

The geometry and steric hindrance of the two *t*-butyl groups of the guanidine catalyst will determine how the two reactants (*i.e.* phosphinic acid and nitrostyrene) align in the C–P bond forming transition state. Due to the bifunctional mode of activation, the guanidine catalyst is expected to interact with both reactants simultaneously *via* hydrogen bonds in the transition state. To gain access to the β carbon for the nucleophilic attack, the C–P forming bond length is estimated to be ~2.3 Å, derived from C···P distance in the uncatalyzed transition state (Fig. S1, ESI†). Based on these two geometrical requirements together with the steric constraint imposed by the two bulky *t*-butyl groups, the two reactants are most likely to align in opposite faces of the bicyclic ring plane in **TS2**. Two possible alignments are envisaged: A and B (Fig. 6).

Various possible conformations of **TS2** were then obtained by varying the dihedral angle of the C–P forming bond, *i.e.* the 4 atoms of both unsaturated carbons on nitrostyrene and the phosphorus and oxygen atoms on phosphinic acid, systematically while keeping the dual hydrogen bonds with the catalyst. For both alignments A and B, nitrostyrene can form hydrogen bond with the guanidine N–H proton with either oxygen atom of the nitro group: s-*cis* or s-*trans* with respect to the C=C double bond (Fig. 7), which exposes the *Re* or *Si* face, respectively, for the nucleophilic attack. A total of 4 *R*-inducing (*R*-**TS2a–d**) and 4 *S*-inducing (*S*-**TS2g–j**) transition states were located. The optimized geometries of these 8 **TS2** transition states are given in Fig. 8. The stability of various transition states is determined predominately by the hydrogen bonding interactions and the steric repulsion with the catalyst and these factors essentially influence the final enantiomeric outcome of the catalytic phospha–Michael reaction.

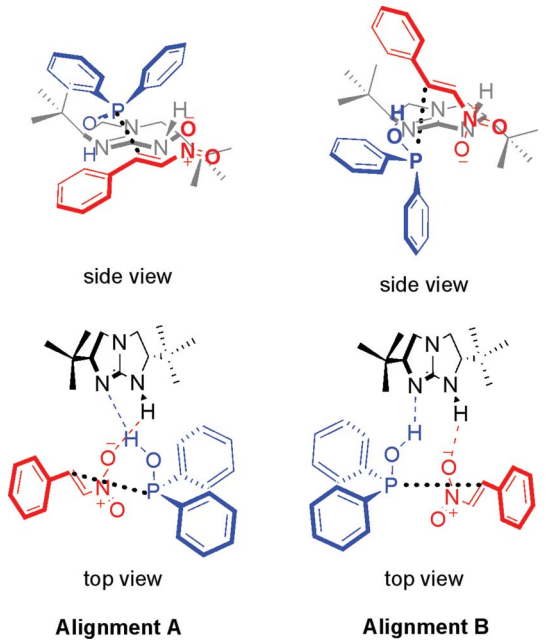

Fig. 6 Two possible alignments of reactants, alignment A and B, in transition state **TS2**. Proximity to the catalyst is not shown to scale.

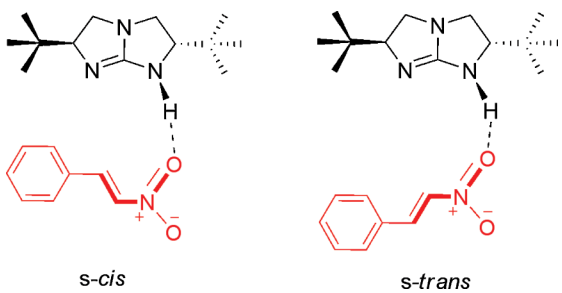

Fig. 7 Two possible modes of hydrogen bonding between nitrostyrene and the guanidine catalyst.

Transition states with alignment B (Fig. 6) is expected to be less favourable as both nitrostyrene and phosphinic acid will encounter greater steric hindrance within the range of the nucleophilic attack (see Fig. S2, ESI†). Moreover, the bulky phosphinic acid is in the plane where there is severe steric interaction. As a result, the hydrogen bonds between the catalyst and both reactants are compromised. Furthermore, the geometry of the guanidine N–H proton causes the nitrostyrene in alignment B to be further away from the range of the phosphinic acid where its steric repulsion is minimized. This is exemplified by comparing *R*-**TS2a** (with alignment A) and *S*-**TS2i** (with alignment B) (see Fig. S3, ESI†). The reactants encounter greater steric interactions with the catalyst in order to achieve the proximity required for the transition state in *S*-**TS2i**, which leads to its energetic instability when compared to *R*-**TS2a**. For instance, the closest H···H distances between the catalyst and nitrostyrene are 2.75 and 2.40 Å for *R*-**TS2a** and *S*-**TS2i**.

For transition state with alignment A, the selectivity of *Re* or *Si* face is determined mainly by which oxygen atom is involved in the hydrogen bond of nitrostyrene with the catalyst. The two different modes of nitrostyrene hydrogen bonding are coined s-*cis* and s-*trans* (Fig. 7) with respect to the single bond between the conjugating α,β unsaturated double bond and the binding N–O bond. In the case of s-*trans* hydrogen bond, the electrophilic β- carbon is significantly further away from the nucleophilic phosphorus atom. For both reactants to stay within the range

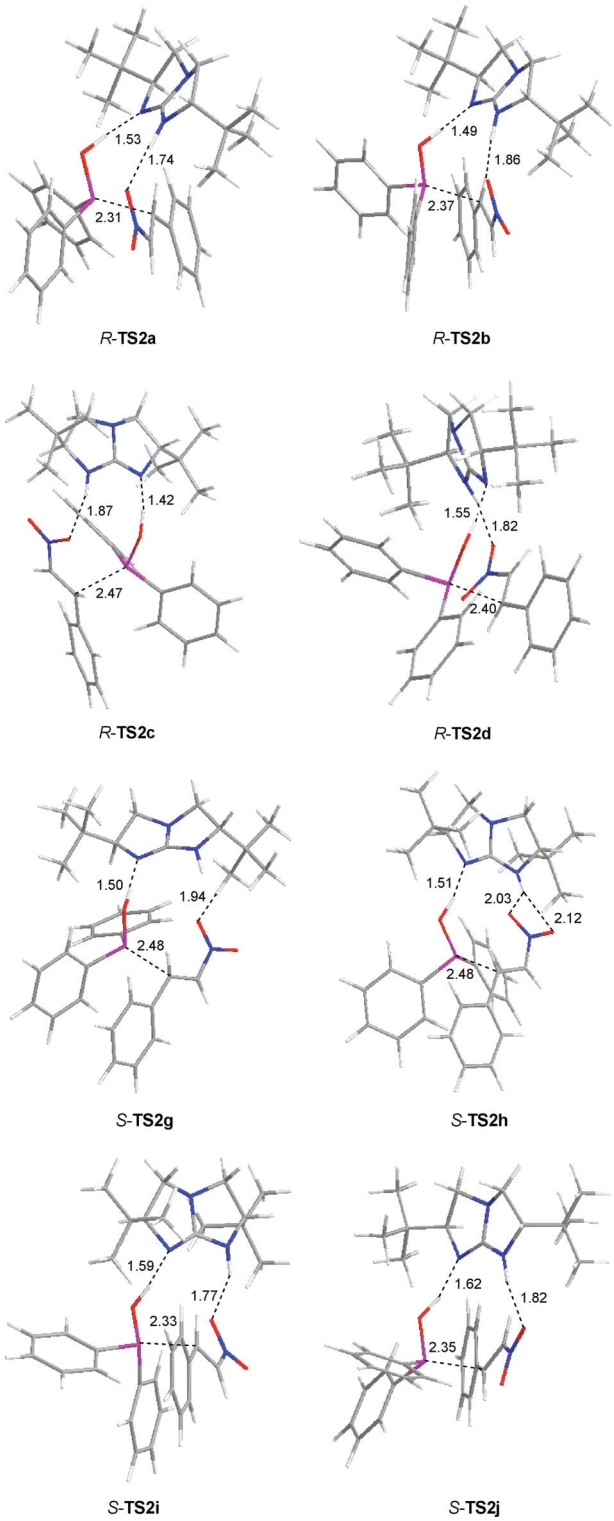

Fig. 8 Optimized (M06-2X/cc-pVDZ) geometries of various *R*- and *S*-forming transition states of **TS**. Hydrogen bond and C···P forming bond distances are given in Å.

of nucleophilic attack (*i.e.* C–P bond formation) in the transition state, either the phosphinic acid or nitrostyrene moiety has to move to a less favourable position (see Fig. S4, ESI†). Either of these geometry adjustments will lead to weakening of the hydrogen bonds and result in a less stable transition state. This difference is illustrated by comparing *S*-**TS2j** and *R*-**TS2a**, where both transition states adopt alignment A but with different modes of nitrostyrene hydrogen bonding. *S*-**TS2j** adopts the s-*trans* nitrostyrene hydrogen bonding and the phosphinic acid has a significantly longer hydrogen bond length than that in *R*-**TS2a** (1.62 *vs.* 1.53 Å). The same trend is observed for the hydrogen bond length of the nitrostyrene with the catalyst (1.81 *vs.* 1.74 Å). Furthermore, the β-carbon is less accessible to the phosphorus in transition states with s-*trans* hydrogen bond. *S*-**TS2j** is less stable than *R*-**TS2a** by 26 kJ mol^{-1}. The preference for s-*cis* nitrostyrene hydrogen bond and the favorable orientation of reactants in alignment A lead to the preference of *Re* face attack. Thus, *R*-**TS2a** which possesses such geometry is the lowest in energy among the various **TS2** conformations considered.

Morokuma–Kitaura energy decomposition analysis (EDA)[24] was employed here to examine the type and magnitude of intermolecular interactions between two substrate moieties. This approach has been applied to various systems to quantify the intermolecular interactions, include water molecules, inorganic and organic molecules[29a–d] and even proteins.[29e] The trend in the Morokuma energy decomposition analysis (Table S3–S5, ESI†) of the 2 most stable *R*- and *S*-inducing transition states confirms the preference of alignment A and s-*cis* nitrostyrene hydrogen bonding. Here, the dispersion energy is estimated by taking the difference between the Hartree–Fock and the MP2 energies. As evidenced in Table S3,† the total interaction energies between the reactants and the catalyst, with both reactants treated as one monomer, correlates well with the trend of the stability of the transition state. The polarization and charge transfer interaction energies can be attributed to the hydrogen bonding interactions as the filled orbital of one monomer donates to the empty orbital of the other (charge transfer) or within itself (polarization). Transition states with alignment A (*i.e.* *R*-**TS2a** and *S*-**TS2h**) have greater polarization and charge transfer interaction energies when compared to those with alignment B (*i.e.* *R*-**TS2d** and *S*-**TS2i**). This trend in polarization and charge transfer interaction energies is further confirmed in the energy decomposition analysis of phosphinic acid with the catalyst (Table S4†), where nitrostyrene is removed in the transition state and the tautomer is treated as a monomer. The important role of the nitrostyrene hydrogen bonding mode in stabilizing the transition state is modeled by using nitrostyrene as a monomer (with phosphinic acid moiety removed from the transition state) and computed its interaction with the guanidine catalyst (Table S5†). Polarization and charge transfer interaction energies are significantly stronger for *R*-**TS2a** and *S*-**TS2i** (with s-*cis* hydrogen bond) compared to *R*-**TS2d** (with s-*trans* hydrogen bond).

In summary, the most favourable calculated transition states correspond to the formation of *R* enantiomer, in pleasing accord with the observed enantioselectivity.[9] Among all the transition states examined, *R*-**TS2a** has the lowest activation energy, $\Delta G^{\ddagger}_{233}$ = 43.0 kJ mol^{-1} with respect to phosphine oxide + nitrostyrene + guanidine catalyst (Fig. 9). The trend of the computed relative

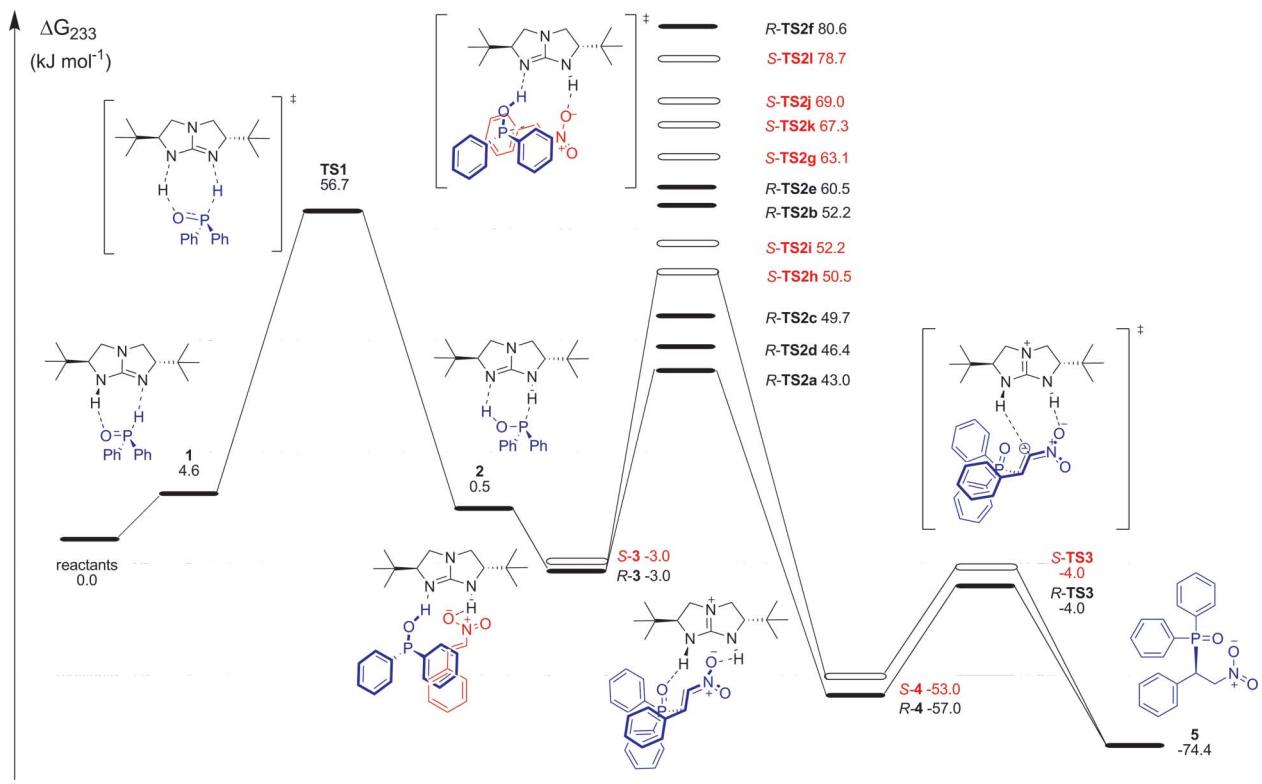

Fig. 9 Schematic energy profile of the cyclic guanidine-catalyzed phospha–Michael reaction between phosphorus oxide and nitrostyrene. Solid bars signify the *R* stereochemistry while hollow bars signify *S* stereochemistry. Calculated relative free energies in diethyl ether solvent were obtained at SMD-M06-2X/cc-pVTZ//M06-2X/cc-pVDZ level.

free energies of various **TS2** transition states (Fig. 9) correlates well with the experimental finding that the bicyclic guanidine-catalyzed phospha–Michael reaction favours the *R* enantiomer.[9] The lowest *S*-inducing transition state (*i.e.* *S*-**TS2e**) lies 7 kJ mol^{-1} higher in energy than *R*-**TS2a**. Finally, we note that transition states with only one reactant form hydrogen bond with the catalyst, namely *R*-**TS2e**, *R*-**TS2f**, *S*-**TS2l** and *S*-**TS2k** (Fig. S5, ESI†), are significantly higher in energy that those with dual hydrogen bonds with the catalyst (Fig. 9). This clearly demonstrates the importance of the bifunctionality of the bicyclic guanidine catalyst.

Intermolecular hydrogen bonds in TS2 transition states

To further shed light on the hydrogen bonding interactions in various *R*-**TS2** and *S*-**TS2** transition states (Fig. 8), topological analysis based on Bader's theory of atoms in molecules (AIM)[21] was carried out. The AIM theory allows one to identify and characterize a bonding interaction between atoms through an analysis of the charge density ρ. The AIM analysis has been successfully employed to characterize hydrogen bonds and non-covalent interactions in a variety of molecular complexes, including hydrogen-bonded complexes.[30] In AIM topological analysis, hydrogen bond is characterized by a bond critical point (bcp) between the interacting hydrogen and hydrogen acceptor. The charge density value (ρ) at the bond critical point is low, compared to typical covalent bond.[30a] In addition, the Laplacian of the charge density ($\nabla^2\rho$) at bcp is characterized by a positive value (represented closed-shell interaction), in contrast to the negative $\nabla_2\rho$ of a typical covalent bond.[30a] The calculated ρ and $\nabla^2\rho$ values at the bond critical points of various hydrogen bonds in *R*-**TS2** and *S*-**TS2** transition states are summarized in Table S6.† As evidenced this Table, the $\nabla_2\rho$ values are positive, consistent with systems with a typical hydrogen bond. The charge density (ρ) at the bond critical point is in the range 0.007–0.035, an order of magnitude smaller than those with typical covalent bonds.[30a] Several theoretical studies have shown that the electron density ρ can be used to quantify the strength of the hydrogen bond.[31] Hence, the ρ value provides a useful indicator of the strength of hydrogen bond in the transition states. For most of the **TS2** transition states examined, nitrostyrene hydrogen bonded to the guanidine catalyst. The trend of hydrogen bonding interaction is reflected in the computed ρ values in Table S6.† The strongest N–H$\cdots$O hydrogen bond occurs in *R*-**TS2a**, which is the most stable C–P bond forming transition state. Other key hydrogen bond involves interaction between oxygen lone pair of nitrostyrene with phosphinic acid proton. As evidenced in Table S6,† other weaker C–H$\cdots$X interactions are also present, such as aromatic C–H (from phosphinic acid) interaction with the nitrostyrene, *t*-butyl C–H interaction with the nitro group or the phosphinic acid O moiety and vinylic or aromatic C–H (from nitrostyrene) interaction with the catalyst basic N moieties. These weaker but significant hydrogen bonds will aid in the stabilization of the transition state and are important in understanding the relative stability of various transition states. Overall, the hydrogen bond between nitrostyrene and the guanidine N–H moiety is a critical factor in governing the stability of the enantioselective step of concerted C–P bond forming and deprotonation transition state (**TS2**).

Proton transfer from guanidine catalyst to nitronate intermediate

In the final stage of the catalytic cycle, abstraction of the N–H proton from the guanidine catalyst by the nucleophilic α carbon of the nitronate yields the final Michael addition product. The transition states leading to *R* and *S* enantiomers are *R*-**TS3** and *S*-**TS3**, respectively. In the nitronate guanidinium complex **4**, there is a monodentate hydrogen bond between the phosphine oxide moiety and the nitro group. The geometry of complex **4** sets up the proximity for the proton transfer. Both transition states *R*-**TS3** and *S*-**TS3** are close in energies. This final proton transfer step is predicted to have a significantly lower activation barrier than the previous C–P bond forming step (see schematic energy diagram Fig. 9). This clearly shows that this final step does not have a major energetic effect on the stereochemical outcome of the phospha–Michael product. In both *R*-**TS3** and *S*-**TS3**, the N–H proton of the catalyst forms hydrogen bond with the nitro group of the nitrostyrene moiety (see Fig. 10).

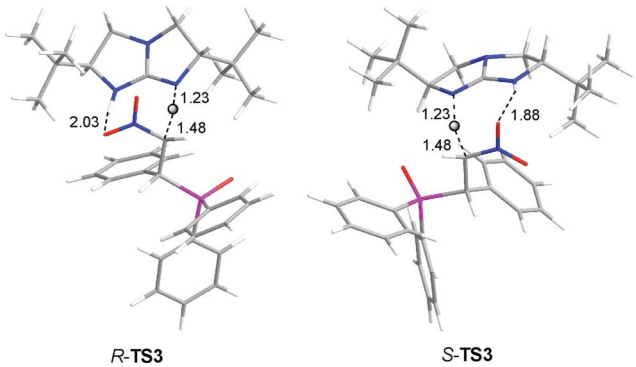

Fig. 10 Optimized (M06-2X/cc-pVTZ) geometries of the transition states *R*-**TS3** and *S*-**TS3** for the third stage of the catalytic cycle. Hydrogen bond and C$\cdots$H forming bond distances are given in Å.

Conclusions

DFT calculations have been employed to investigate the mechanism of the phospha–Michael reaction between phosphine oxide and nitrostyrene using the bicyclic guanidine catalyst. The bicyclic guanidine catalyst is found to play a dual activation mode role in all 3 key stages of the proposed catalytic cycle (Fig. 1). It acts as a Brønsted base and a Brønsted acid simultaneously in the transition states. In the first stage, the bicyclic guanidine catalyst facilitates the tautomerization of phosphine oxide to phosphinic acid. The enantioselective and rate determining step for the carbon-phosphorus bond formation occurs in the second stage. The phosphinic acid tautomer serves as the nucleophile (Michael donor) for the enantioselective step. The calculated activation barriers for the formation of *R*- and *S*-products correlate well with the experimental observation that *R*-enantiomer is the preferred product. Hydrogen bonding and steric interactions between the nitrostyrene and the catalyst are essential factors in governing the stability of the various transition states. The origin of enantioselectivity can be understood in terms of the geometry that can be adopted in the catalyst cavity. This finding is supported by the calculated activation barriers, transition state geometries and hydrogen bonding analysis based on AIM

analysis. In the final stage of the catalytic cycle, the guanidine catalyst facilitates the abstraction of the N–H proton from the catalyst by the nucleophilic α carbon of the nitronate. Overall, the bicyclic guanidine catalyst serves an essential role in lowering the activation barrier through its bifunctional capability and asymmetric induction *via* its chirality.

Acknowledgements

This work was supported by ARF grant (R-143-000-342-112) from the National University of Singapore (NUS). We also thank the NUS Medicinal Chemistry programme for their generous financial support.

Notes and references

1 (*a*) L. Albrecht, A. Albrecht, H. Krawczyk and K. A. Jorgensen, *Chem.–Eur. J.*, 2010, **16**, 28–48; (*b*) D. Enders, A. Saint-Dizier, M.-I. Lannou and A. Lenzen, *Eur. J. Org. Chem.*, 2006, 29–49.
2 (*a*) W. S. Wadsworth Jr. and W. D. Emmons, *J. Am. Chem. Soc.*, 1961, **83**, 1733–1738; (*b*) B. H. Lipshutz, D. W. Chung, B. Rich and R. Corral, *Org. Lett.*, 2006, **8**, 5069–5072; (*c*) M. Shi and Y.-H. Liu, *Org. Biomol. Chem.*, 2006, **4**, 1468–1470.
3 (*a*) N. T. McDougal and S. E. Schauls, *J. Am. Chem. Soc.*, 2003, **125**, 12094–12095; (*b*) Y. K. Chung and G. C. Fu, *Angew. Chem., Int. Ed.*, 2009, **48**, 2225–2227.
4 (*a*) T. Akiyama, J. Itoh, K. Yokota and K. Fuchibe, *Angew. Chem., Int. Ed.*, 2004, **43**, 1566–1568; (*b*) M. Rueping, A. P. Antonchick and T. Theissmann, *Angew. Chem., Int. Ed.*, 2006, **45**, 3683–3686; (*c*) S. Hoffmann, A. M. Seayad and B. List, *Angew. Chem., Int. Ed.*, 2005, **44**, 7424–7427; (*d*) S. Hoffmann, M. Nicoletti and B. List, *J. Am. Chem. Soc.*, 2006, **128**, 13074–13075; (*e*) M. Kawasaki and H. Yamamoto, *J. Am. Chem. Soc.*, 2006, **128**, 16482–16483; (*f*) S. J. Connon, *Angew. Chem., Int. Ed.*, 2006, **45**, 3909–3912.
5 (*a*) W. Tang and X. Zhang, *Chem. Rev.*, 2003, **103**, 3029–3070; (*b*) S. H. Hong, D. P. Sander, C. W. Lee and R. H. Grubbs, *J. Am. Chem. Soc.*, 2005, **127**, 17160–17161; (*c*) R. T. Yu, E. E. Lee, G. Malik and T. Rovis, *Angew. Chem. Int. Ed.*, 2009, **48**, 2379–2382; (*d*) C. Nájera and J. M. Sansano, *Angew. Chem., Int. Ed.*, 2009, **48**, 2452–2456.
6 (*a*) F. Palacios, C. Alonso and J. M. Santos, *Chem. Rev.*, 2005, **105**, 899–931; (*b*) J. G. Allen, F. R. Atherton, M. J. Hall, C. H. Hassall, S. W. Homles, L. W. Lambert, L. J. Nisbet and P. S. Ringrose, *Nature*, 1978, **272**, 56–58; (*c*) S. Fushimi, K. Furihata and H. Seto, *J. Antibiot (Tokyo)*, 1989, **42**, 1019–1025.
7 (*a*) D. Leow and C.-H. Tan, *Chem.–Asian J.*, 2009, **4**, 488–507; (*b*) D. Leow and C.-H. Tan, *Synlett*, 2010, **11**, 1589–1605.
8 M. P. Coles, *Chem. Commun.*, 2009, 3659–3676.
9 X. Fu, Z. Jiang and C.-H. Tan, *Chem. Commun.*, 2007, 5058–5060.
10 (*a*) J. Shen, T. T. Nguyen, Y. P. Goh, W. Ye, X. Fu, J. Xu and C.-H. Tan, *J. Am. Chem. Soc.*, 2006, **128**, 13692–13693; (*b*) W. Ye, Z. Jiang, Y. Zhao, L. M. S. Goh, D. Leow, Y.-T. Soh and C.-H. Tan, *Adv. Synth. Catal.*, 2007, **349**, 2454–2458; (*c*) Z. Jiang, W. Ye, Y. Yang and C.-H. Tan, *Adv. Synth. Catal.*, 2008, **350**, 2345–2351; (*d*) Z. Jiang, Y. Yang, Y. Pan, Y. Zhao, H. Liu and C.-H. Tan, *Chem.–Eur. J.*, 2009, **15**, 4925–4930; (*e*) D. Leow, S. Lin, S. K. Chittimalla, X. Fu and C.-H. Tan, *Angew. Chem., Int. Ed.*, 2008, **47**, 5641–5645; (*f*) H. Liu, D. Leow, K.-W. Huang and C.-H. Tan, *J. Am. Chem. Soc.*, 2009, **131**, 7212–7213.
11 Z. Jiang, Y. Pan, Y. Zhao, T. Ma, R. Lee, Y. Yang, K.-W. Huang, M. W. Wong and C.-H. Tan, *Angew. Chem., Int. Ed.*, 2009, **48**, 3627–3631.
12 (*a*) M. K. Kiesewetter, M. D. Scholten, N. Kirn, R. L. Weber, J. L. Hedrick and R. M. Waymouth, *J. Org. Chem.*, 2009, **74**, 9490–9496; (*b*) A. Chuma, H. W. Horn, W. C. Swope, R. C. Pratt, L. Zhang, B. G. G. Lohmeijer, C. G. Wade, R. M. Waymouth, J. L. Hedrick and J. E. Rice, *J. Am. Chem. Soc.*, 2008, **130**, 6749–6754; (*c*) L. Simón and J. M. Goodman, *J. Org. Chem.*, 2007, **72**, 9656–9662.
13 P. Hammar, C. Ghobril, C. Antheaume, A. Wagner, R. Baati and F. Himo, *J. Org. Chem.*, 2010, **75**, 4728–4736.
14 E. J Corey and M. J. Grogan, *Org. Lett.*, 1999, **1**, 157–160.
15 J. Li, W.-Y. Jiang, K.-L. Han, G.-Z. He and C. Li, *J. Org. Chem.*, 2003, **68**, 8786–8789.
16 R. Lee, X. Lim, T. Chen, G. K. Tan, C.-H. Tan and K.-W. Huang, *Tetrahedron Lett.*, 2009, **50**, 1560–1562.
17 (*a*) Y. Zhao and D. G. Truhlar, *Theor. Chem. Acc.*, 2008, **120**, 215–241; (*b*) Y. Zhao and D. G. Truhlar, *Acc. Chem. Res.*, 2008, **41**, 157–167.
18 (*a*) T. H. Dunning Jr., *J. Chem. Phys.*, 1989, **90**, 1007–1023; (*b*) R. A. Kendall, T. H. Dunning Jr. and R. J. Harrison, *J. Chem. Phys.*, 1992, **96**, 6796–6806.
19 (*a*) Y. Zhao and D. G. Truhlar, *Chem. Phys. Lett.*, 2011, **502**, 1–13; (*b*) V. Vrcek and H. Mestric, *J. Phys. Org. Chem.*, 2009, **22**, 59–68; (*c*) K. Wakamatsu, A. Orita and J. Otera, *Organometallics*, 2010, **29**, 1290–1295; (*d*) A. C. Voukides, K. M. Konrad and R. P. Johnson, *J. Org. Chem.*, 2009, **74**, 2108–2113.
20 A. V. Marenich, C. J. Cramer and D. G. Truhlar, *J. Phys. Chem. B*, 2009, **113**, 6378–6396.
21 R. F. W. Bader, *Atoms in Molecules - A Quantum Theory*, Oxford Science Publications, Oxford, 1990.
22 P. L. A. Popelier, R. G. A. Bone, *MORPHY98*, UMIST, Manchester, 1998 .
23 M. J. Frisch, G. W. Trucks, H. B. Schlegel, G. E. Scuseria, M. A. Robb, J. R. Cheeseman, G. Scalmani, V. Barone, B. Mennucci, G. A. Petersson, H. Nakatsuji, M. Caricato, X. Li, H. P. Hratchian, A. F. Izmaylov, J. Bloino, G. Zheng, J. L. Sonnenberg, M. Hada, M. Ehara, K. Toyota, R. Fukuda, J. Hasegawa, M. Ishida, T. Nakajima, Y. Honda, O. Kitao, H. Nakai, T. Vreven, J. A. Montgomery, Jr., J. E. Peralta, F. Ogliaro, M. Bearpark, J. J. Heyd, E. Brothers, K. N. Kudin, V. N. Staroverov, R. Kobayashi, J. Normand, K. Raghavachari, A. Rendell, J. C. Burant, S. S. Iyengar, J. Tomasi, M. Cossi, N. Rega, J. M. Millam, M. Klene, J. E. Knox, J. B. Cross, V. Bakken, C. Adamo, J. Jaramillo, R. Gomperts, R. E. Stratmann, O. Yazyev, A. J. Austin, R. Cammi, C. Pomelli, J. W. Ochterski, R. L. Martin, K. Morokuma, V. G. Zakrzewski, G. A. Voth, P. Salvador, J. J. Dannenberg, S. Dapprich, A. D. Daniels, O. Farkas, J. B. Foresman, J. V. Ortiz, J. Cioslowski and D. J. Fox, *Gaussian 09 (Revision A.1)*, Gaussian, Inc., Wallingford CT, 2009.
24 K. Kitaura and K. Morokuma, *Int. J. Quantum Chem.*, 1976, **10**, 325–340.
25 M. W. Schmidt, K. K. Baldridge, J. A. Boatz, S. T. Elbert, M. S. Gordon, J. H. Jensen, S. Koseki, N. Matsunaga, K. A. Nguyen, S. Su, T. L. Windus, M. Dupuis and J. A. Montgomery, *J. Comput. Chem.*, 1993, **14**, 1347–1363.
26 (*a*) I. Schlemminger, Y. Saida, H. Groger, W. Maison, N. Durot, H. Sasai, M. Shibasaki and J. Martens, *J. Org. Chem.*, 2000, **65**, 4818–4825; (*b*) D. B. Chestnut, *Heteroat. Chem.*, 2000, **11**, 73–80.
27 Y. V. Babin and Y. A. Ustynyuk, *Russian J. Phys. Chem. A*, 2007, **81**, 2017–2027.
28 T. Isobe, K. Fukuda, K. Yamaguchi, H. Seki, T. Tokunaga and T. Ishikawa, *J. Org. Chem.*, 2000, **65**, 7779–7785.
29 (*a*) H. Umeyama and K. Morokuma, *J. Am. Chem. Soc.*, 1977, **99**, 1316–1332; (*b*) K. Kitaura and K. Morokuma, in *Molecular Interactions*, ed. H. Ratajczak and W. J. Orville-Thomas, Wiley, Chichester, England, 1980, vol. 1; (*c*) K. Morokuma and K. Kitaura, in *Chemical Applications of Atomic and Molecular Electrostatic Potentials*, ed. P. Politzer and D. G. Truhlar, Plenum, New York, 1981, p. 215; (*d*) M. S. Gordon and J. H. Jensen, in *Encyclopedia of Computational Chemistry*, ed. P. V. R. Schleyer, Wiley, Chichester, England, 1998, vol. 5; (*e*) J. Wang, J. Gut and J. Leszczynski, *J. Phys. Chem. B*, 2005, **109**, 13761–13769.
30 (*a*) U. Koch and P. L. A. Popelier, *J. Phys. Chem.*, 1995, **99**, 9747–9754; (*b*) A. Vila, R. A. Mosquera and J. M. Hermida-Ramon, *THEOCHEM*, 2001, **541**, 149–158; (*c*) S. Wojtulewski and S. J. Grabowski, *THEOCHEM*, 2003, **621**, 285–291; (*d*) B. Schiøtt, B. B. Iversen, G. K. H. Madsen, F. K. Larsen and T. C. Bruice, *Proc. Natl. Acad. Sci. U. S. A.*, 1998, **95**, 12799–12802.
31 (*a*) R. Jiong and M. W. Wong, *Aust. J. Chem.*, 2009, **62**, 1062–1067; (*b*) O. Knop, R. J. Boyd and S. Choi, *J. Am. Chem. Soc.*, 1988, **110**, 7299–7301; (*c*) R. F. W. Bader, T.-H. Tang, Y. Tal and F. W. Biegler-Konig, *J. Am. Chem. Soc.*, 1982, **104**, 946–952; (*d*) S. J. Grabowski, *Chem. Phys. Lett.*, 2001, **338**, 361–366.